Cyclooxygenase-2 Mediates Anandamide Metabolism in the Mouse Brain

Sherrye T. Glaser and Martin Kaczocha

Departments of Neurobiology and Behavior (S.T.G.) and Biochemistry and Cell Biology (M.K.), Stony Brook University, Stony Brook, New York

ABSTRACT

Cyclooxygenase-2 (COX-2) mediates inflammation and contributes to neurodegeneration. Best known for its pathological up-regulation, COX-2 is also constitutively expressed within the brain and mediates synaptic transmission through prostaglandin synthesis. Along with arachidonic acid, COX-2 oxygenates the endocannabinoids anandamide (AEA) and 2-arachidonoylglycerol in vitro. Inhibition of COX-2 enhances retrograde signaling in the hippocampus, suggesting COX-2 mediates endocannabinoid tone in healthy brain. The degree to which COX-2 may regulate endocannabinoid metabolism in vivo is currently unclear. Therefore, we explored the effect of COX-2 inhibition on [³H]AEA metabolism in mouse brain. Although AEA is hydrolyzed primarily by fatty acid amide hydrolase (FAAH), ex vivo autoradiography revealed that COX-2 inhibition by nimesulide redirected [³H]AEA substrate from COX-2 to FAAH in the cortex, hippocampus, thalamus, and periaqueductal gray. These data indicate that COX-2 possesses the capacity to metabolize AEA in vivo and can compete with FAAH for AEA in several brain regions. Temporal fluctuations in COX-2 expression were observed in the brain, with an increase in COX-2 protein and mRNA in the hippocampus at midnight compared with noon. COX-2 immunolocalization was robust in the hippocampus and several cortical regions. Although most regions exhibited no temporal changes in COX-2 immunolocalization, increased numbers of immunoreactive cells were detected at midnight in layers II and III of the somatosensory and visual cortices. These temporal variations in COX-2 distribution reduced the enzyme's contribution toward [³H]AEA metabolism in the somatosensory cortex at midnight. Taken together, our findings establish COX-2 as a mediator of regional AEA metabolism in mouse brain.

Introduction

Cyclooxygenase-2 (COX-2) produces prostaglandins through oxygenation of arachidonic acid. Numerous functions and pathological phenomena have been attributed to the products of COX-2 in the central nervous system. Most notably, COX-2 is up-regulated in response to excitotoxicity or tissue damage. This pathological process leads to an increase in prostaglandin levels and additional neuronal damage (for review, see Yang and Chen, 2008).

In healthy nervous systems, COX-2 is constitutively expressed with localization primarily in the hippocampus, cortex, and amygdala (Yamagata et al., 1993). On a subcellular level, COX-2 immunoreactivity (IR) is primarily in the perikarion and proximal dendrites (Yamagata et al., 1993).

Electron microscopy studies localized rat brain COX-2 to endomembranes in dendrites near synaptic inputs from axon terminals (Wang et al., 2005).

Constitutive COX-2 activity and expression mediates long-term potentiation (LTP) in mice (Chen et al., 2002) and rats (Slanina et al., 2005; Akaneya and Tsumoto, 2006) and long-term depression in rats (Murray and O'Connor, 2003). The promotion of LTP by COX-2 probably results from prostaglandin E_2 activation of the prostaglandin E_2 receptor, because N-(4-nitro-2-phenoxyphenyl)methanesulfonamide (nimesulide)-induced reductions of LTP in the mouse dentate gyrus can be rescued by administering prostaglandin E_2 (Chen et al., 2002), and receptor gene suppression reduces LTP in the visual cortex (Akaneya and Tsumoto, 2006). Overall, COX-2's localization pattern, along with its association with synaptic plasticity, suggests a major role for this enzyme in the processes of learning and memory (for review, see Yang and Chen, 2008).

In addition to metabolizing arachidonic acid, COX-2 oxygenates endocannabinoids, producing prostamides and pros-

ABBREVIATIONS: COX-2, cyclooxygenase-2; AEA, anandamide; FAAH, fatty acid amide hydrolase; IR, immunoreactivity; LTP, long-term potentiation; 2-AG, 2-arachidonoylglycerol; MGL, monoglyceride lipase; qRT-PCR, quantitative real-time polymerase chain reaction; PAG, periaqueductal gray; PBST, phosphate-buffered saline Tween 20; CAY10397, 5-[[4-(ethoxycarbonyl)phenyl]azo]-2-hydroxy-benzeneacetic acid.

taglandin glycerol esters (Yu et al., 1997; Kozak et al., 2002). This discovery is not surprising, because endocannabinoids are structurally similar to arachidonic acid, and the omega fatty acid portion of molecules from both groups interacts effectively with amino acids in COX-2's active site (Kozak et al., 2003).

Although the endogenous production of oxygenated endocannabinoid products by COX-2 is well documented, the functions of these recently discovered signaling molecules and their receptor targets are still being elucidated. The first study showing a signaling role for an oxygenated endocannabinoid reported that prostaglandin E_2 glycerol ester, an oxidative metabolite of 2-arachidonoylglycerol (2-AG), significantly increased miniature inhibitory postsynaptic current frequency in cultured hippocampal neurons (Sang et al., 2006). In a subsequent publication, the same authors showed in hippocampal cultures that prostaglandin E_2 glycerol ester enhances excitatory glutamatergic synaptic transmission and promotes neurodegeneration (Sang et al., 2007). To date, it is not known what receptor compounds such as prostaglandin E_2 glycerol ester activate. It is interesting to note, however, that these oxidative products act in direct opposition to endocannabinoids, which have long been shown to exhibit neuroprotective effects (for review, see Galve-Roperh et al., 2008).

Although COX-2 metabolizes endocannabinoids, it is widely accepted that endogenous cannabinoids are hydrolyzed primarily by fatty acid amide hydrolase (FAAH) and monoglyceride lipase (MGL). FAAH is widely distributed throughout the mouse brain (Egertová et al., 2003) and efficiently metabolizes the endocannabinoids anandamide (AEA) and 2-AG. Transgenic mice lacking FAAH possess elevated endogenous AEA levels, suggesting that FAAH is the principal metabolizing enzyme of AEA in the mouse (Cravatt et al., 2001; Lichtman et al., 2002). Another article has demonstrated that activity-dependent changes in AEA tone mediate the selective "local tuning" of hippocampal inhibitory synapses (Kim and Alger, 2010). The observed changes in AEA tone were regulated by fluctuations in local FAAH activity. Like FAAH, MGL is widely expressed in the brain (Dinh et al., 2002) and metabolizes 2-AG but not AEA (Long et al., 2009).

Although COX-2 is not considered a major endocannabinoid-metabolizing enzyme, the oxygenation of endocannabinoids is physiologically important, because COX-2 inhibition potentiates rat hippocampal 2-AG signaling (Kim and Alger, 2004). Therefore, COX-2 probably regulates hippocampal endocannabinoid tone and may compete with FAAH and/or MGL for endocannabinoid substrates.

In this study, we used a novel ex vivo FAAH imaging technique (Glaser et al., 2006) and the selective COX-2 inhibitor nimesulide to examine whether endogenous COX-2 activity competes with FAAH for [^{3}H]AEA metabolism in the brains of live mice. A previous report identified nimesulide as having no effect on FAAH activity (Fowler et al., 2003). We examined 11 brain regions to expand on prior work (Kim and Alger, 2004; Slanina and Schweitzer, 2005) that was restricted to hippocampal neurons possessing high endogenous expression of COX-2, FAAH, and MGL. In addition, we analyzed temporal changes in COX-2 expression and localization in mouse brains by conducting experiments at the midpoint of the light and dark cycles and studied whether temporal

changes in COX-2 distribution affected regional [^{3}H]AEA metabolism.

Materials and Methods

Animals. C57BL/6 mice (Taconic Farms, Germantown, NY) weighing approximately 25 g were kept in light/dark 12:12 h. Mice were studied at the midpoint of the light and dark cycles. All mice were maintained with free access to food and water according to federal guidelines for the care and use of animals. These studies followed international guidelines on the ethical use of animals in research, with animal numbers and their suffering kept to a minimum. These studies were approved by the Institutional Review Committee.

Regional COX-2 Western Blots. At the midpoints of the light and dark periods, regional brain dissections were performed on six mice at each time point, and tissue was homogenized in chilled Tris + 1 mM EDTA + complete Mini EDTA acid-free protease inhibitor cocktail (Roche Diagnostics, Mannheim, Germany). Once protein concentrations were determined by bicinchoninic acid protein assay (Pierce Chemical, Rockford, IL), samples (40 µg of protein/lane) were run on a 10% SDS-polyacrylamide gel electrophoresis gel. After transfer to a nitrocellulose membrane at 100 V for 25 min, blots were blocked in 5% nonfat dry milk in phosphate-buffered saline Tween 20 (PBST) for 1 h and probed for 1 h with polyclonal rabbit COX-2 antibody directed against amino acids 584 to 598 of murine COX-2 (Cayman Chemical, Ann Arbor, MI) at a final concentration range of 1:100 to 1:400 or monoclonal mouse anti-β actin antibody directed against amino acids 1 to 14 of *Xenopus laevis* actin (Abcam, Inc. Cambridge, MA) at a final concentration of 1:20,000. The blots were rinsed three times with PBST followed by incubation with goat anti-mouse or goat anti-rabbit IgG horseradish peroxidase-conjugated antibodies (Molecular Probes, Eugene, OR) for 1 h. After three rinses with PBST, blots were developed by using the Immun-star horseradish peroxidase substrate (Bio-Rad Laboratories, Hercules, CA) and exposed to film. Temporal changes in regional COX-2 protein levels were determined by normalizing COX-2 levels to β-actin levels within the same lane and comparing samples by densitometry using ImageJ software (http://rsbweb.nih.gov/ij). Significance was determined by unpaired two-tailed t test using Prism 4 (GraphPad Software Inc., San Diego, CA).

COX-2 Immunolocalization. Wild-type C57BL/6 mice were kept at light/dark 12:12 h. Six hours after the onset of the light or dark periods (noon and midnight, respectively), mice were deeply anesthetized and perfused with 3% formaldehyde in saline. Brains were isolated and postfixed for another 4 h in 3% formaldehyde, then cryoprotected in 30% sucrose. Fixed brains were embedded in 3% gelatin and 30% egg albumin and frozen in liquid nitrogen-cooled isopentane. For all immunofluorescence studies, noon and midnight cryosections (10 µm thick) were run simultaneously. Statistical analysis (Table 1) and compared samples were processed at the same time. Six mice were used for each time point. Sections were rinsed, blocked for 20 min in 2% normal goat serum, and incubated overnight at 4°C in the rabbit anti-COX-2 diluted 1:150. After washing in PBS, tissue was blocked again and incubated with donkey-anti-rabbit-fluorescein isothiocyanate (1:800) (Jackson ImmunoResearch Laboratories, Inc., West Grove, PA) for 35 min at 37°C.

Slides were rinsed then coverslipped with Vectashield (Vector Laboratories, Burlingame, CA). Sections were observed with a Zeiss epifluorescence microscope (Carl Zeiss Inc., Thornwood, NY) with filter sets that were optimized for fluorescein isothiocyanate viewing. Controls for COX-2 IR were prepared both by omitting the primary antibody and after overnight preadsorption of the COX-2 antiserum with a 10-fold molar excess of the immunizing peptide antigen.

In Vitro COX-2 Activity Time Course for Determining Nimesulide Bioavailability. Mouse brains were isolated 15, 30, and 45 min after the intraperitoneal administration of 25 mg/kg

TABLE 1
Quantification of COX-2 IR profiles in cortical laminae of the somatosensory and visual cortices

COX-2 IR soma in cortical laminae II/ III and V/ IV were tallied in representative visual fields of 0.0339 mm² in mouse brains isolated at both noon and midnight. In a double-blind analysis, the ratio of immunoreactive profiles in each group of laminae were calculated for each visual field, and the average ratios and standard error were calculated for noon and midnight conditions. Three visual fields from each mouse were analyzed, and six mice were examined. Significance was determined by analysis of variance. Relative to noon, there was a higher average number of immunoreactive profiles in laminae II and III at midnight and fewer COX-2 IR profiles in laminae V and VI. This caused the ratio of immunoreactive profiles in laminae II and III / laminae V and VI to significantly (** $P < 0.01$) shift in a positive direction from noon to midnight, indicating a shift in the population of immunoreactive profiles in these cortical regions.

Time of Day	Average Number of COX-2 IR Profiles Lamina II/III	Average Number of COX-2 IR Profiles Lamina V/VI	Ratio Lamina II/III Lamina V/VI
Noon	39.8 ± 1.8	37.7 ± 5.9	1.20 ± 0.12
Midnight	57.2 ± 3.9	26.9 ± 2.4	2.20 ± 0.14**

nimesulide (Cayman Chemical) in 1:4:5 ethanol/alkamus 620 (Rhone-Poulenc, Princeton, NJ)/saline and immediately homogenized on ice. Control homogenates were from mice administered vehicle only. Three mice were used in each condition. Homogenates were normalized for protein levels and assayed for tissue nimesulide levels with an in vitro COX-2 activity assay (a modified version of a previously published protocol; Kalgutkar et al., 1998). Human recombinant COX-2 (Cayman Chemical) (11 units per sample) was preincubated on ice for 30 min in 100 mM Tris-HCl buffer + 1 mM EDTA, pH 8.0, with 0.47% phenol, 1 μM hematin, 40 μM 5-[[4-(ethoxycarbonyl)phenyl]azo]-2-hydroxy-benzeneacetic acid (CAY10397) (a selective prostaglandin dehydrogenase inhibitor), and 225 mg of brain homogenate. After the preincubation, 23.3 nCi of [1–14C]arachidonic acid (PerkinElmer Life and Analytical Sciences, Waltham, MA) and 1 μM unlabeled arachidonic acid were added to each tube (final volume = 300 μl), and samples were transferred to a 37°C shaker water bath for 10 min. The incubation was terminated upon the addition of chilled diethyl ether/methanol/1 M citrate (30:4:1), pH 4.0, containing butylated hydroxyanisole (an antioxidant) (10 mg) and unlabeled arachidonic acid (10 mg). Samples were centrifuged, and the organic phase was spotted on a thin-layer chromatography plate (Amersham, Arlington Heights, IL). Thin-layer chromatography was run at 4°C in a mobile phase consisting of ethyl acetate/dichloromethane (methylene chloride)/acetic acid (75:25:1). Each sample lane was cut into 1-cm squares. Each square was added to a tube containing scintillation fluid, and the total radioactivity was determined by scintillation counting. The inhibition of prostanoid generation by nimesulide present in the homogenates was compared between control samples and homogenates generated at various times after nimesulide administration. Significance was determined by paired two-tailed t test using Excel (Microsoft, Redmond, WA). Data were graphed with Prism 4 (GraphPad Software Inc.).

In Vitro FAAH Enzyme Activity Assays. Six hours after the onset of the light and dark periods, regional brain dissections were performed on six mice for each time point. After tissue homogenization in Tris + 1 mM EDTA on ice, protein concentrations were determined by bicinchoninic acid protein assay (Pierce Chemical). FAAH activity assays were performed according to published methods (Deutsch and Chin, 1993). In brief, 300 μg of regional homogenate, 500 μg of fatty acid-free bovine serum albumin, 100 μM AEA (Cayman Chemical) plus 0.22 μCi arachidonoyl ethanolamide [ethanolamine-1-3H] (a generous gift from the National Institute on Drug Abuse, Bethesda, MD) were incubated in Tris + 1 mM EDTA, pH 7.6 at 37°C in triplicate for 15 min while shaking. The reactions were terminated by the addition of two volumes of 1:1 chloroform/methanol. Samples were centrifuged, and the aqueous phase was measured by liquid scintillation counting. The rates of AEA hydro-

lysis per milligram of protein per hour were compared between noon and midnight regional homogenates. Data were graphed and significance was determined by unpaired two-tailed t test with a Bonferroni's correction using Prism 4 (GraphPad Software Inc.).

Ex Vivo Autoradiography of Brain FAAH Activity. Radiolabeled AEA [arachidonoyl 5,6,8,9,11,12,14,15-3H] was a generous gift from the National Institute on Drug Abuse Drug Inventory Supply Program. AEA (Cayman Chemical), and [3H]AEA were dissolved in a 1:1:18 mixture of ethanol/alkamus-620/saline. Mice were intravenously administered 1 mg/kg AEA + 2 mCi/kg [3H]AEA. Fifteen minutes after injection, mice were sacrificed, and their brains were promptly transferred to a beaker containing iced saline to minimize further diffusion and protein-mediated processes. Half of the cerebellum and a blood sample were homogenized, extracted in 1:1 chloroform/methanol, and analyzed by scintillation counting and thin-layer chromatography (solvent system was 6:3:1 ethyl acetate/hexane/acetic acid; Deutsch and Chin, 1993) to quantify total tritium accumulation and [3H]AEA breakdown in these tissues. Chilled brains were transferred into iced 2% formaldehyde + 2% glutaraldehyde in phosphate buffer for 1 h. The brains were then washed three times with iced phosphate buffer and cryoprotected at 4°C in 30% sucrose in phosphate buffer. Serial 15-μm cryosections were generated, and images were acquired for 10 h by using a BetaImager (Biospace Mesures, Paris, France).

Autoradiography Analysis. Serial sections were analyzed, and surface radioactivity (cpm/mm²) in regions of interest was quantified by using BetaVision+ image analysis software (Biospace Mesures). Data were entered into Excel (Microsoft), and average regional tritium accumulation/mm², representing AEA and its metabolites, was determined. Six mice were used for each condition. Regional surface activities of each mouse were normalized by dividing the activity of each region over that of the pontine nuclei (the region of lowest tritium accumulation) of the same mouse. Normalization enabled regional comparison among animals with slightly different levels of brain tritium uptake. Standard error was calculated by using Excel. Data were graphed, and one-way analysis of variance with Dunnett's post test was performed to determine significance between noon and midnight samples by using Prism 4 (Graph Pad Software Inc.).

Quantitative Real-Time Polymerase Chain Reaction. At the midpoint of the light and dark periods, regional dissections were performed on six mice and RNA was extracted by using the RNeasy mini kit (QIAGEN, Valencia, CA). One microgram of RNA was subjected to cDNA synthesis by using the Superscript III first strand synthesis kit (Invitrogen, Carlsbad, CA). Quantitative real-time polymerase chain reaction (qRT-PCR) analysis was performed by using the StepOne Plus Real-Time PCR system (Applied Biosystems, Foster City, CA) and the following primers: COX-2 (forward: 5′-AGGACTGGGCCATGGAGT-3′ and reverse: 5′-ACCTCTCCACCAATGACCTG-3′) and β-actin (forward: 5′-GACGGCCAGGTCATCACTAT-3′ and reverse: 5′-CGGATGT-CAACGTCACACTT-3′). Each 20-μl reaction (performed in triplicate) contained cDNA, 100 nM primer mix, and 10 μl of Power SYBR Green PCR Master Mix (Applied Biosystems). The cycling conditions were as follows: 95°C for 10 min, followed by 40 cycles at 95°C for 15 s and 60°C for 60 s. Negative controls lacking cDNA were included for all reactions. Amplification levels were determined by using the ΔΔCt method with β-actin serving as the housekeeping gene.

Results

Temporal Changes in COX-2 Distribution. The regional distribution of COX-2 was compared at noon and midnight by Western blot (Fig. 1). A control Western blot against whole brain homogenate showed one band at ∼75 kDa, which was not detected in cerebellar homogenates or in whole brain homogenates after preadsorption with immunizing peptide
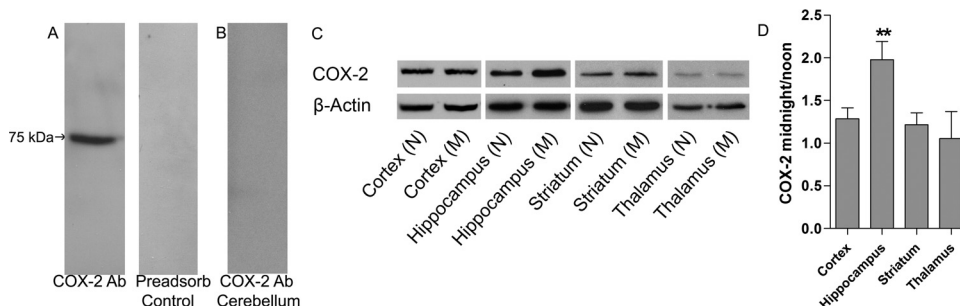
Fig. 1. Regional COX-2 Western blots. Homogenates were generated from brains from six mice isolated at the midpoint of the light (noon; N) and dark (midnight; M) cycles and probed for COX-2 IR. A, whole brain homogenate produces a single 75-kDa band that is blocked when the membrane is preincubated with immunizing peptide. B, cerebellar homogenates lack COX-2 IR. C, regional expression levels of COX-2 with β-actin serving as the endogenous control are shown. D, regional COX-2 levels were quantified by densitometry of Western blots, and midnight and noon conditions were compared. Expression levels were normalized to β-actin and subsequently analyzed. The data presented in the graph represents regional normalized midnight densitometry/normalized noon densitometry. Bars represent the regional mean ± S.E. Significance was determined by an unpaired two-tailed t test. An increase in COX-2 protein levels was observed in hippocampal homogenates. ∗∗, $p < 0.05$.

(Fig. 1, A and B). Brains were harvested at the midpoint of the light and dark cycles, and regional dissections were performed. The cortex, hippocampus, striatum, and thalamus were homogenized and analyzed by Western blot. All regions were COX-2-immunoreactive, with the cortex and hippocampus exhibiting the most immunoreactivity (Fig. 1C). Increases in COX-2 protein levels were observed in midnight hippocampal samples ($p < 0.05$) (Fig. 1D). qRT-PCR corroborated the elevated expression of COX-2 in midnight hippocampi ($p < 0.05$) compared with noon samples (Fig. 2). COX-2 mRNA was also detected in cortical, striatal, and thalamic samples, although their levels did not vary ($p > 0.05$) with a temporal pattern.

As temporal changes in COX-2 protein and mRNA levels were detected, we performed immunohistochemistry on brains collected at noon and midnight to detect potential temporal changes in COX-2-immunoreactive cell populations. COX-2 IR was most robust in the hippocampus and various cortical regions, including the piriform cortex, so-
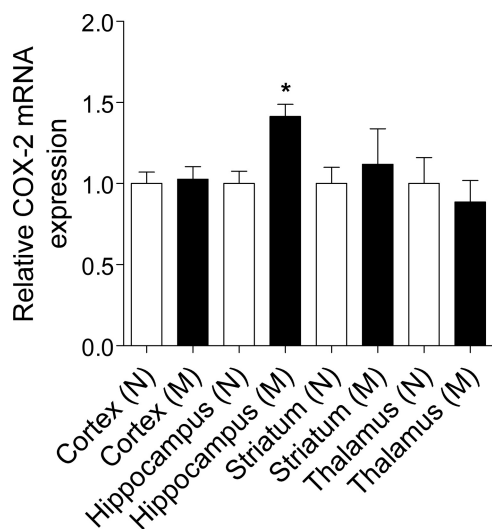
matosensory cortex, and visual cortex (Fig. 3). In the somatosensory and visual cortices (Fig. 3, 1N–4M), COX-2 IR was observed in laminae II, II, V, and VI. Comparing noon and midnight brain samples, changes in COX-2 IR cortical populations were observed, with a higher ($p < 0.01$) ratio of immunoreactive profiles in laminae II/III relative to laminae V/VI in midnight somatosensory cortex and visual cortex samples (Table 1). Therefore, although COX-2 expression does not increase in the cortex, COX-2 distribution in the somatosensory and visual cortices changes, with additional profiles exhibiting COX-2 IR at midnight.

Several other brain regions exhibited robust COX-2 IR, including the piriform cortex (Fig. 3, 5N and 5M), hippocampus (Fig. 3, 6N–8M), and amygdala (Fig. 3, 9N and 9M). In the hippocampus (Fig. 3, 6N–8M), COX-2 IR was concentrated in CA2 and CA3, with little immunoreactivity observed in the dentate gyrus or CA1. Both the piriform cortex and CA2 and CA3 of the hippocampus seemed to have increased COX-2 IR at midnight. Although COX-2 expression and protein levels were detected in the striatum and thalamus (Figs. 1 and 2), COX-2 IR was too diffuse to reliably analyze in these regions. Likewise, no COX-2 IR was detected in the periaqueductal gray (PAG) (data not shown).

COX-2 Competes with FAAH for [³H]AEA Substrate. COX-2 is known to oxidize endogenous AEA and 2-AG (Yu et al., 1997; Kozak et al., 2002), and its inhibition potentiates cannabinoid receptor signaling in the hippocampus (Kim and Alger, 2004). Therefore, we performed the first study to estimate the contribution of COX-2 activity toward global AEA metabolism in the mouse brain by using an ex vivo autoradiography approach that quantifies regional [³H]AEA metabolism by FAAH in intact brains (Glaser et al., 2006).

The Ex Vivo Autoradiography Trapping Mechanism. The assay used here quantifies local FAAH activity in intact tissue by measuring the accumulation of tritiated arachidonic acid ([³H]AA) trapped in membranes after [³H]AEA hydrolysis. After the intravenous administration of [³H]AEA, tracer enters the brain and is metabolized by local enzymes, including FAAH and COX-2 (Fig. 4). In the case of FAAH, [³H]AEA is rapidly hydrolyzed, producing [³H]AA, which is promptly incorporated into cellular membranes. If the tracer is instead oxygenated by COX-2, [³H]prostamide is produced. Unlike FAAH metabolites, prostamides escape entrapment in cellular membranes
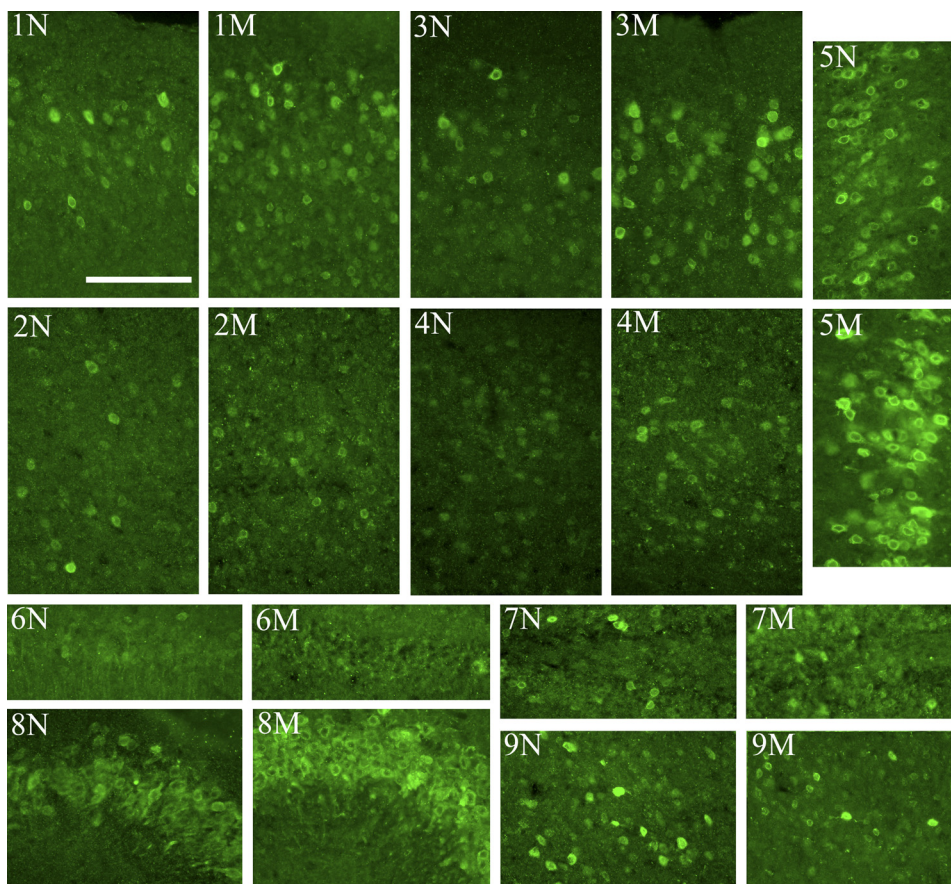

Fig. 2. qRT-PCR analysis of COX-2 expression in brains at noon (N) and midnight (M). Six mouse brains were dissected, and the cortex, hippocampus, striatum, and thalamus were subjected to RNA extraction, cDNA synthesis, and qRT-PCR analysis. Relative mRNA levels were determined with β-actin serving as the housekeeping gene. The mRNA expression levels of each region were normalized to the respective noon samples. Values represent means of at least five independent experiments performed in triplicate. ∗, $p < 0.05$.

Fig. 3. Distribution of COX-2 IR in the mouse brain at noon (N) and midnight (M). Mice were perfused, and six brains were isolated at the midpoint of their light (noon) and dark (midnight) cycles. Brains were sectioned and processed for immunofluorescence studies by using a primary polyclonal antibody directed against mouse COX-2. COX-2 IR was prominent throughout the cortex (1–4) and hippocampus (6–8), with additional immunoreactivity observed in the amygdala (9). In the cortex, layers II/III of the somatosensory (1N) and visual (3N) cortices exhibited robust COX-2 IR likely in pyramidal cells at noon, and layers V/VI of the somatosensory (2N) and visual (4N) cortices displayed very modest COX-2 IR. Relative to noon samples, COX-2 IR increased in layers II/III of the somatosensory (1M) and visual (3M) cortices at midnight and remained similar to the noon samples in layers V/VI of the somatosensory (2M) and visual (4M) cortices. The piriform cortex (5N and 5M) had extensive COX-2 IR at both time points with a slight increase in the intensity of immunoreactivity in midnight samples (5M). In the hippocampus, COX-2 IR was very low in CA1 (6N and 6M) and the dentate gyrus (7N and 7M) at both time points, with CA2 and CA3 (8N and 8M) exhibiting the majority of COX-2 IR soma in that region. CA2 and CA3 also exhibited a possible increase in fluorescence at midnight (8M) relative to noon (8N), suggesting a potential increase in hippocampal COX-2 at that time point. The amygdala (9N and 9M) contained a modest number of COX-2 IR soma that did not seem to substantially change between noon and midnight. Scale bar, 50 μm.
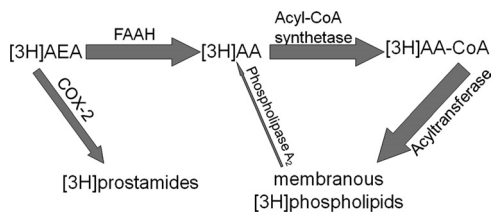

Fig. 4. Trapping mechanism for [³H]AEA metabolites is shown. After [³H]AEA administration, [³H]AEA enters the brain and undergoes either hydrolysis by FAAH or oxygenation by COX-2. Upon hydrolysis by FAAH, [³H]AEA is converted into [³H]AA, which is promptly incorporated into cellular membranes. This membranous tritium is easily imaged by ex vivo autoradiography and quantified. Upon oxygenation by COX-2, the [³H]prostamide freely diffuses throughout the tissue.

and are able to freely diffuse throughout the tissue. As a result, [³H]AEA metabolism by FAAH produces an increase in regional tritium levels, and metabolism by COX-2 results in no change in regional tritium levels. However, if both enzymes are coexpressed, [³H]AEA metabolism by COX-2 would reduce local [³H]AEA availability to FAAH, thereby reducing the accumulation of tritiated FAAH metabolites in that region. As a result, if COX-2 and FAAH are competing locally for [³H]AEA substrate, this autoradiography assay will detect a reduction in regional tritium accumulation.

Nimesulide Administration Inhibits COX-2 but Not FAAH in the Brain. To discern between FAAH and COX-2 activity, we imaged brains after intraperitoneal administration of vehicle or nimesulide, a selective competitive COX-2 inhibitor. Before conducting brain imaging studies, we determined the degree of nimesulide penetration into

the brain after intraperitoneal administration with an in vitro COX-2 activity assay. We harvested brains 15 to 45 min after the intraperitoneal administration of 25 mg/kg nimesulide or vehicle. Endogenous COX-2 activity in healthy brain was too low to detect by in vitro enzymatic assays (data not shown). In contrast, purified COX-2 activity was readily detectable. Therefore, the presence of nimesulide in brains was determined by the brain homogenates' ability to inhibit purified COX-2 in an in vitro activity assay. Purified COX-2 activity was significantly reduced ($p < 0.05$) by nimesulide-treated homogenates that were generated at least 30 min after intraperitoneal administration. In sharp contrast, control samples and homogenates generated 15 min after nimesulide administration did not affect ($p > 0.05$) purified COX-2 activity (Fig. 5). These data indicate that ample nimesulide had entered the brain under the assay conditions selected for the autoradiography experiments. We next conducted in vitro FAAH activity assays using the same nimesulide-treated and control homogenates. We detected no difference in regional activity between control and nimesulide-treated samples (Fig. 6). Collectively, these results indicate that COX-2, but not FAAH, will be inhibited in autoradiography experiments performed 30 min after nimesulide administration.

Ex Vivo Autoradiography. We used autoradiography to examine the impact of COX-2 inhibition on regional [³H]AEA metabolism by FAAH at noon and midnight. Both nimesulide- and vehicle-treated brains exhibited robust tritium accumulation, especially in the cortex and hippocampus (Fig. 7). At noon, nimesulide treatment dramat-
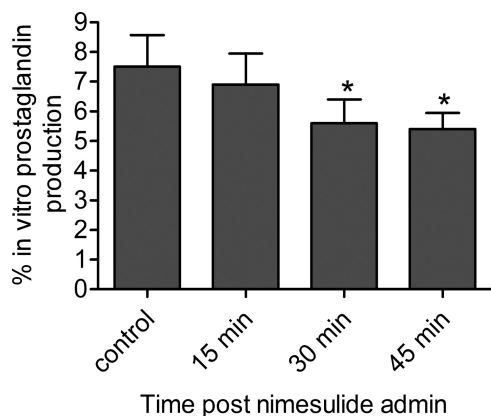
Fig. 5. Nimesulide accumulates in the brain after intraperitoneal administration. Mice were intraperitoneally administered vehicle or 25 mg/kg nimesulide, and their brains were isolated 0, 15, 30, and 45 min later. Three mice were included at each time point. To detect the presence of nimesulide in brain, purified COX-2 enzyme was added to brain homogenates of vehicle- or nimesulide-injected mice, and the samples were tested for their ability to oxygenate [^{14}C]AA. Relative to control samples, homogenates generated 30 and 45 min after nimesulide administration exhibited significantly ($p < 0.05$) less [^{14}C]prostaglandin generation, indicating that a substantial quantity of nimesulide accumulated in brain by these time points.
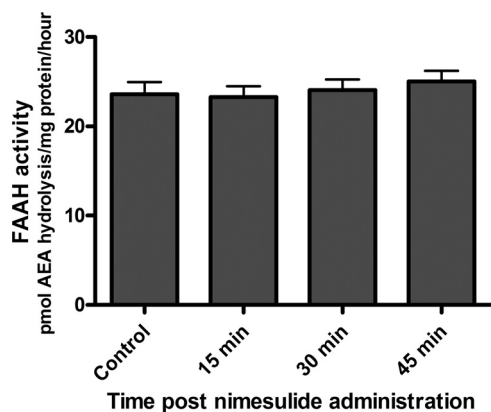

Fig. 6. Regional FAAH activity is not affected by nimesulide administration. Wild-type mice were intraperitoneally administered vehicle or 25 mg/kg nimesulide, and their brains were isolated 0, 15, 30, and 45 min later. Homogenates were generated, and FAAH activity was determined. [^{3}H]AEA hydrolysis in control and nimesulide-treated homogenates was similar ($p > 0.05$), indicating that nimesulide treatment does not alter regional FAAH activity in the brain.

ically elevated ($p < 0.05$) tritium accumulation in the hippocampus, somatosensory cortex, piriform cortex, thalamus, and PAG without affecting the other brain regions examined (Fig. 8A). At midnight, nimesulide treatment similarly increased ($p < 0.05$) tritium accumulation in the hippocampus, somatosensory cortex, thalamus, and piriform cortex. Midnight control and nimesulide-treated brains exhibited similar levels of tritium in the PAG ($p > 0.05$) (Fig. 8B), suggesting reduced metabolism of [^{3}H]AEA by COX-2 at midnight relative to noon. Compared with control samples, nimesulide significantly ($p < 0.05$) altered tritium accumulation in the somatosensory cortex at both noon and midnight. However, by comparing the two time points, it was discovered that nimesulide treatment exhibited significantly less effect ($p < 0.05$) at midnight relative to noon.

Discussion

In the brain, COX-2 mediates synaptic transmission by synthesizing neuromodulatory prostaglandins (for review, see Yang and Chen, 2008). Here, we report that COX-2 is capable of metabolizing the endocannabinoid AEA in vivo. Our ex vivo imaging method unmasked an unexpectedly robust contribution by COX-2 toward global AEA metabolism in the mouse brain, thereby ascribing functional significance for COX-2 in endocannabinoid metabolism.

This is the first study to describe the influence of regional COX-2 activity on AEA hydrolysis by FAAH. Unlike traditional enzyme assays using tissue homogenates, our ex vivo imaging method is ideally suited for the study of two enzymes competing for substrate at the regional level. We used nimesulide, a selective COX-2 inhibitor (see Figs. 5 and 6), to discern [^{3}H]AEA metabolism by FAAH and COX-2. As described earlier, tracer metabolism by FAAH produces [^{3}H]AA, which is promptly trapped in cellular membranes. Unlike [^{3}H]AA, COX-2 metabolites are expected to escape such trapping mechanisms and freely diffuse throughout the brain. Therefore, regions with significant COX-2 [^{3}H]AEA metabolism will, upon nimesulide administration, instead shunt [^{3}H]AEA toward FAAH, resulting in increased [^{3}H] arachidonic acid being trapped in regional membranes. After nimesulide administration, we observed increased tritium accumulation at both noon and midnight in the hippocampus, thalamus, piriform cortex, and somatosensory cortex (Fig. 8). Nimesulide administration also caused an increase in noon PAG tritium accumulation. These data suggest that competition between FAAH and COX-2 for AEA may serve as a point of regulation for brain AEA signaling in numerous regions.

Competition for substrate necessitates close proximity between enzymes within the same brain region. As expected, the COX-2 IR pattern in C57BL/6 mice is similar to both the distribution of COX-2 in rat brains (Yamagata et al., 1993; Wang et al., 2005) and the distribution of FAAH in C57BL/6 mice (Egertová et al., 2003). Both COX-2 IR (Fig. 3) and FAAH IR (Egertová et al., 2003) are found throughout the cortex, with prominent immunoreactivity in the piriform cortex and layers II and III of the somatosensory and visual cortices. In the hippocampus, both COX-2 and FAAH IR exhibit robust immunoreactivity, although COX-2 IR is concentrated primarily in CA2 and CA3. FAAH IR was also prominent in most thalamic nuclei. Although COX-2 IR was not detected in this region (Fig. 3), both COX-2 protein (Fig. 1) and mRNA (Fig. 2) were detected, suggesting low levels of the enzyme exist in the thalamus. It is noteworthy that regions consistently exhibiting nimesulide-dependent increases in tritium accumulation (Fig. 8) express both COX-2 and FAAH (Egertová et al., 2003). These data suggest that FAAH and COX-2 are sufficiently colocalized to compete for [^{3}H]AEA substrate in these brain regions.

The autoradiography assay used here more closely mimics endogenous AEA metabolism than in vitro enzyme assays providing an excess of substrate. Through autoradiography analysis, regions with robust COX-2 expression, such as the hippocampus, exhibit no more dramatic differences between control and COX-2-inhibited states than the thalamus. Similar to in vivo settings where endogenous AEA levels are produced in limited quantities, these results are probably caused by limited substrate/tracer availability restricting
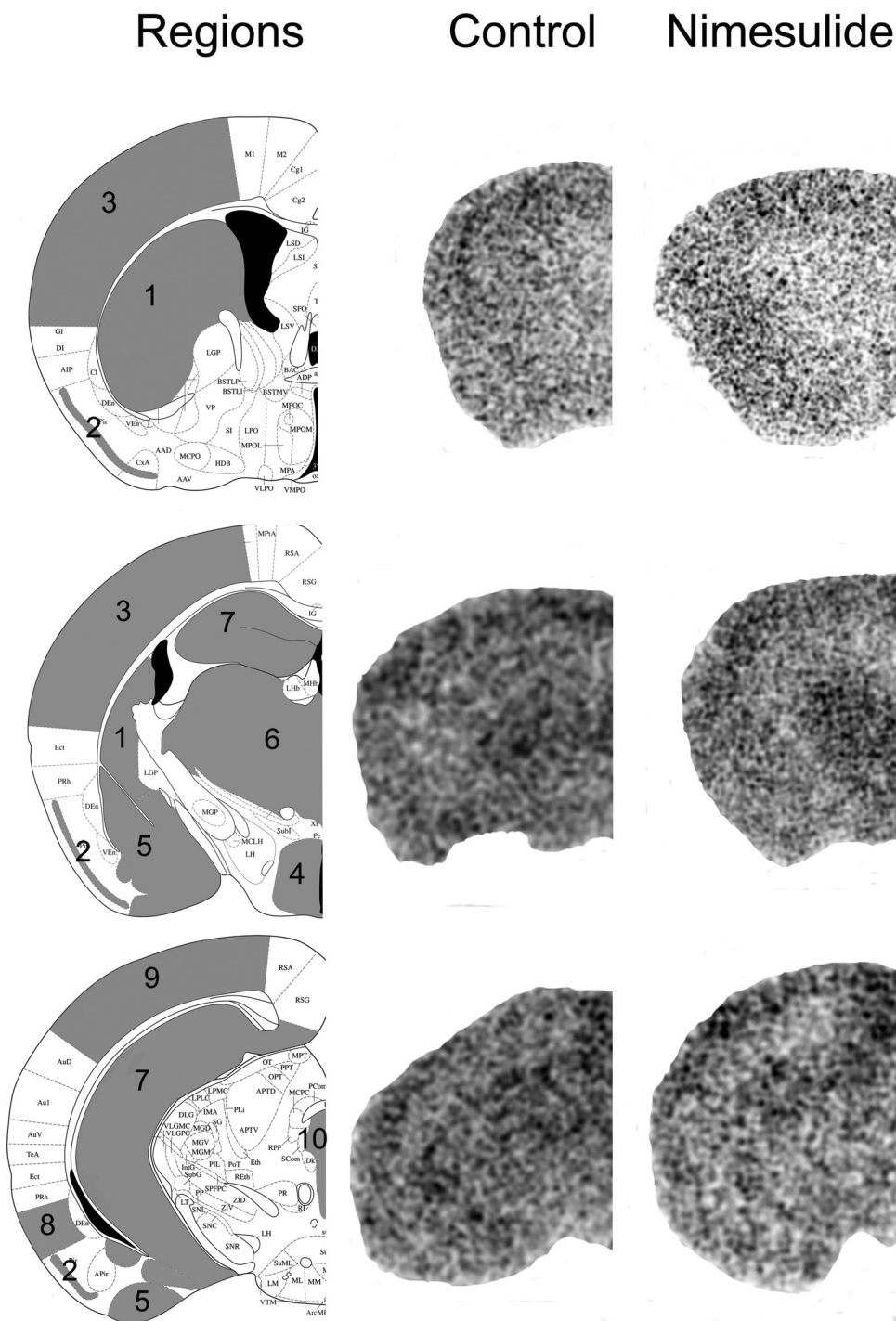
Regions   Control   Nimesulide

Fig. 7. Regional tritium distribution in control and nimesulide-treated mice. After the administration of 25 mg/kg nimesulide or vehicle, mice were administered 1 mg/kg + 50 µCi [³H]AEA, and their brains were processed for ex vivo autoradiography. Left, a schematic of the regions pictured in the autoradiographs (center and right). Analyzed regions are depicted in gray and include the (1) caudate putamen, (2) the piriform cortex, (3) the somatosensory cortex, (4) the hypothalamus, (5) the amygdala, (6) the thalamus, (7) the hippocampus, (8) the entorhinal cortex, (9) the visual cortex, (10) the PAG, and the cerebellum. [³H]AEA and its metabolites accumulated in a heterogeneous pattern in both control (center) and nimesulide-treated brains (right), with the most accumulation observed in the cortical and thalamic regions. The images that are modified at left were originally published in Paxinos and Franklin, 2001 (plates 32, 44, and 54).

COX-2 activity in control animals. These results suggest that COX-2 is expressed in several brain regions at levels in excess of what is required to metabolize endogenous substrates such as AEA, possibly to ensure the prompt metabolism of these lipid signaling molecules and prevent their accumulation near receptors.

To date, all physiology studies that show COX-2's influence over endogenous cannabinoid signaling have studied the hippocampus (Kim and Alger, 2004; Slanina and Schweitzer, 2005), the brain region exhibiting the most robust COX-2 expression. Our data reveal that even regions with modest COX-2 expression can exhibit competi-

tion between COX-2 and FAAH for [³H]AEA substrate. For example, although thalamic COX-2 protein levels are too low to detect by immunofluorescence (Fig. 3), its enzymatic inhibition is sufficient to potentiate [³H]AEA hydrolysis by FAAH. These striking results suggest that COX-2's influence on endocannabionid/endovanilloid signaling could be much more extensive than previously believed and more physiology studies of these systems should be conducted to better ascertain COX-2's influence on these endogenously produced signaling molecules.

Prostamides and prostaglandin glycerol esters have distinct signaling properties from both endocannabinoids and
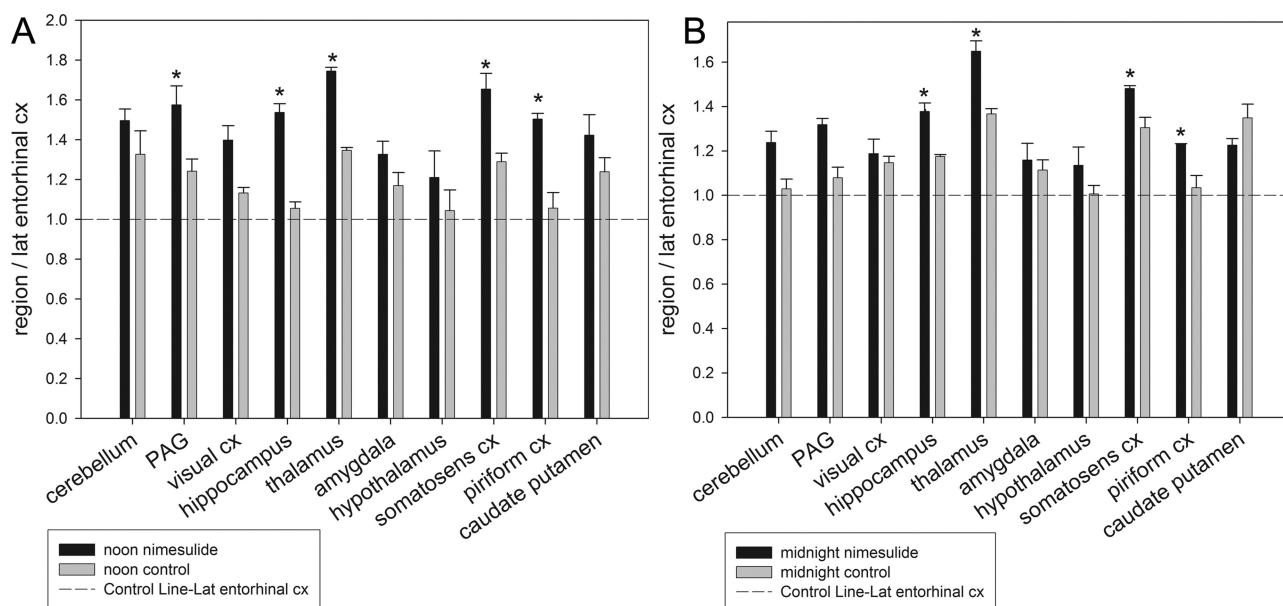
Fig. 8. Ex vivo autoradiography analysis of nimesulide-induced changes in [³H]AEA metabolism by FAAH. Mice were intraperitoneally administered 25 mg/kg nimesulide or vehicle, and 30 min later they were intraperitoneally administered 1 mg/kg AEA + 50 μCi of [³H]AEA at the midpoint of the light (noon) or dark (midnight) cycle. Thirty minutes after tracer administration, brains were isolated, fixed, and processed for imaging in the BetaImager. Six mice were used for each time point. Regional tritium accumulation (cpm/mm²) caused by FAAH activity was quantified by using BetaVision+ software. Regional tritium accumulation was normalized against tritium levels in the lateral entorhinal cortex, a brain region where nimesulide did not alter tritium accumulation, and a region with no detectable COX-2 IR. Normalized regional tritium levels were compared between nimesulide-treated and control samples, and significance was determined by a one-way analysis of variance with Dunnett's post test. Bars represent the regional mean ± S.E. The dotted lines represent the relative value of the lateral entorhinal cortex. A, noon nimesulide-induced changes in regional tritium accumulation. At noon, regional tritium accumulation, representing the accumulation of tritiated FAAH metabolites, was elevated in the PAG, hippocampus, thalamus, somatosensory cortex, and piriform cortex of nimesulide-treated mice relative to control animals (∗, $p < 0.05$). B, midnight nimesulide-induced changes in regional tritium accumulation. Similar to noon, regional tritium accumulation at midnight was higher in the hippocampus, thalamus, somatosensory cortex, and piriform cortex of nimesulide-treated mice relative to control animals (∗, $p < 0.05$).

prostaglandins and do not interact with cannabinoid or prostaglandin receptors (for review, see Woodward et al., 2008). As expected, these compounds have distinct pharmacological properties, with prostamides regulating intraocular pressure (Woodward et al., 2008) and stimulating cat iris contraction (Matias et al., 2004) and glyceryl prostaglandins mediating calcium mobilization, inositol 1,4,5-trisphosphate synthesis, and activation of protein kinase C in RAW264.7 macrophage cells (Nirodi et al., 2004). The data presented in this study suggest that nimesulide can be used to inhibit prostamide production. Not only does this increase substrate availability to FAAH, it also probably could inhibit several prostamide-mediated processes in the body.

We observed temporal changes in COX-2 expression in healthy mouse brains. Relative to noon, Western blot (Fig. 1) and qRT-PCR (Fig. 2) analyses revealed an increase in COX-2 expression in hippocampal samples at midnight. Although the levels of COX-2 protein and mRNA did not vary, immunohistochemistry studies (Fig. 3) detected shifts in immunoreactive cell populations in the somatosensory and visual cortices between noon and midnight with more immunoreactive cells in lamina II and III of midnight samples.

The temporal changes in COX-2 IR observed in the current study were generally too slight to alter the regional distribution pattern of [³H]AEA metabolites between noon and midnight samples (Fig. 8). Only the somatosensory cortex exhibited a significant change between the two time points, with the normalized midnight nimesulide condition exhibiting significantly less effect relative to the noon nimesulide condition. At first glance, the autoradiography data would seem to contradict the immunoreactivity data (Fig. 3) that exhibit an increase in the number of COX-2 IR cells at midnight. However, the pattern of COX-2 IR cells changes in the somatosensory cortex between noon and midnight, and this change in distribution may result in COX-2 becoming more remote from FAAH near specific synaptic connections at midnight, thereby lessening the competition between the two enzymes for substrate.

Similar to COX-2, FAAH exhibits temporal changes in brain expression and activity. In a prior study (Glaser and Kaczocha, 2009), we observed that FAAH activity in the mouse cerebellum and PAG fluctuated temporally, with reductions in regional activity observed in the middle of the dark cycle of the mice. Temporal changes in regional FAAH activity were monitored during this study and were carefully discerned from any nimesulide-induced changes in regional [³H]AEA metabolism. It should be noted that significant reductions in FAAH activity can alter the sensitivity of the autoradiography assay in some brain regions. For example, although PAG tritium accumulation was significantly potentiated by nimesulide at noon, nimesulide exhibited no effect in midnight PAG (Fig. 8). This is probably caused by reduced midnight PAG FAAH activity (Glaser and Kaczocha, 2009) diminishing the sensitivity of the imaging assay in the PAG at midnight.

When results from the current study are grouped with prior reports demonstrating potentiation of 2-AG signaling in the hippocampus after COX-2 inhibition (Kim and Alger, 2004; Slanina and Schweitzer, 2005), the potential regulatory role of COX-2 in endocannabinoid signaling becomes

even more apparent. We predict that systemic nimesulide administration potentiates endogenous AEA signaling in mouse hippocampus, thalamus, somatosensory cortex, piriform cortex, and PAG. It is conceivable that COX-2 also mediates the signaling of other lipid molecules that share similar metabolic pathways to AEA and 2-AG.

In conclusion, this study reveals competition between FAAH and COX-2 for common substrates in multiple brain regions of the mouse. As a result, activity of one enzyme may reduce substrate availability to the other. Just as inhibiting rat hippocampal COX-2 potentiates endocannabinoid signaling (Kim and Alger, 2004; Slanina and Schweitzer, 2005), it is equally likely that FAAH inhibition might potentiate endogenous prostamide signaling within the brain.

References

Akaneya Y and Tsumoto T (2006) Bidirectional trafficking of prostaglandin E_2 receptors involved in long-term potentiation in visual cortex. *J Neurosci* **26:**10209–10221.

Chen C, Magee JC, and Bazan NG (2002) Cyclooxygenase-2 regulates prostaglandin E_2 signaling in hippocampal long-term synaptic plasticity. *J Neurophysiol* **87:**2851–2857.

Cravatt BF, Demarest K, Patricelli MP, Bracey MH, Giang DK, Martin BR, and Lichtman AH (2001) Supersensitivity to anandamide and enhanced endogenous cannabinoid signaling in mice lacking fatty acid amide hydrolase. *Proc Natl Acad Sci USA* **98:**9371–9376.

Deutsch DG and Chin SA (1993) Enzymatic synthesis and degradation of anandamide, a cannabinoid receptor agonist. *Biochem Pharmacol* **46:**791–796.

Dinh TP, Freund TF, and Piomelli D (2002) A role for monoglyceride lipase in 2-arachidonoylglycerol inactivation. *Chem Phys Lipids* **121:**149–158.

Egertová M, Cravatt BF, and Elphick MR (2003) Comparative analysis of fatty acid amide hydrolase and cb(1) cannabinoid receptor expression in the mouse brain: evidence of a widespread role for fatty acid amide hydrolase in regulation of endocannabinoid signaling. *Neuroscience* **119:**481–496.

Fowler CJ, Holt S, and Tiger G (2003) Acidic nonsteroidal anti-inflammatory drugs inhibit rat brain fatty acid amide hydrolase in a pH-dependent manner. *J Enzyme Inhib Med Chem* **18:**55–58.

Galve-Roperh I, Aguado T, Palazuelos J, and Guzmán M (2008) Mechanisms of control of neuron survival by the endocannabinoid system. *Curr Pharm Des* **14:**2279–2288.

Glaser ST and Kaczocha M (2009) Temporal changes in mouse brain fatty acid amide hydrolase activity. *Neuroscience* **163:**594–600.

Glaser ST, Gatley SJ, and Gifford AN (2006) Ex vivo imaging of fatty acid amide hydrolase activity and its inhibition in the mouse brain. *J Pharmacol Exp Ther* **316:**1088–1097.

Kalgutkar AS, Crews BC, Rowlinson SW, Garner C, Seibert K, and Marnett LJ (1998) Aspirin-like molecules that covalently inactivate cyclooxygenase-2. *Science* **280:**1268–1270.

Kim J and Alger BE (2004) Inhibition of cyclooxygenase-2 potentiates retrograde endocannabinoid effects in hippocampus. *Nat Neurosci* **7:**697–698.

Kim J and Alger BE (2010) Reduction in endocannabinoid tone is a homeostatic mechanism for specific inhibitory synapses. *Nat Neurosci* **13:**592–600.

Kozak KR, Gupta RA, Moody JS, Ji C, Boeglin WE, DuBois RN, Brash AR, and Marnett LJ (2002) 15-Lipoxygenase metabolism of 2-arachidonylglycerol. Generation of a peroxisome proliferator-activated receptor α agonist. *J Biol Chem* **277:**23278–23286.

Kozak KR, Prusakiewicz JJ, Rowlinson SW, Prudhomme DR, and Marnett LJ (2003) Amino acid determinants in cyclooxygenase-2 oxygenation of the endocannabinoid anandamide. *Biochemistry* **42:**9041–9049.

Lichtman AH, Hawkins EG, Griffin G, and Cravatt BF (2002) Pharmacological activity of fatty acid amides is regulated, but not mediated, by fatty acid amide hydrolase in vivo. *J Pharmacol Exp Ther* **302:**73–79.

Long JZ, Nomura DK, and Cravatt BF (2009) Characterization of monoacylglycerol lipase inhibition reveals differences in central and peripheral endocannabinoid metabolism. *Chem Biol* **16:**744–753.

Matias I, Chen J, De Petrocellis L, Bisogno T, Ligresti A, Fezza F, Krauss AH, Shi L, Protzman CE, Li C, et al. (2004) Prostaglandin ethanolamides (prostamides): in vitro pharmacology and metabolism. *J Pharmacol Exp Ther* **309:**745–757.

Murray HJ and O'Connor JJ (2003) A role for COX-2 and p38 mitogen activated protein kinase in long-term depression in the rat dentate gyrus in vitro. *Neuropharmacology* **44:**374–380.

Nirodi CS, Crews BC, Kozak KR, Morrow JD, and Marnett LJ (2004) The glyceryl ester of prostaglandin E_2 mobilizes calcium and activates signal transduction in RAW264.7 cells. *Proc Natl Acad Sci USA* **101:**1840–1845.

Paxinos G and Franklin KBJ (2001) *The Mouse Brain in Stereotaxic Coordinates.* Academic Press, San Diego, CA.

Sang N, Zhang J, and Chen C (2006) PGE_2 glycerol ester, a COX-2 oxidative metabolite of 2-arachidonoyl glycerol, modulates inhibitory synaptic transmission in mouse hippocampal neurons. *J Physiol* **572:**735–745.

Sang N, Zhang J, and Chen C (2007) COX-2 oxidative metabolite of endocannabinoid 2-AG enhances excitatory glutamatergic synaptic transmission and induces neurotoxicity. *J Neurochem* **102:**1966–1977.

Slanina KA and Schweitzer P (2005) Inhibition of cyclooxygenase-2 elicits a CB1-mediated decrease of excitatory transmission in rat CA1 hippocampus. *Neuropharmacology* **49:**653–659.

Slanina KA, Roberto M, and Schweitzer P (2005) Endocannabinoids restrict hippocampal long-term potentiation via CB1. *Neuropharmacology* **49:**660–668.

Wang H, Hitron IM, Iadecola C, and Pickel VM (2005) Synaptic and vascular associations of neurons containing cyclooxygenase-2 and nitric oxide synthase in rat somatosensory cortex. *Cereb Cortex* **15:**1250–1260.

Woodward DF, Carling RW, Cornell CL, Fliri HG, Martos JL, Pettit SN, Liang Y, and Wang JW (2008) The pharmacology and therapeutic relevance of endocannabinoid derived cyclo-oxygenase (COX)-2 products. *Pharmacol Ther* **120:**71–80.

Yamagata K, Andreasson KI, Kaufmann WE, Barnes CA, and Worley PF (1993) Expression of a mitogen-inducible cyclooxygenase in brain neurons: regulation by synaptic activity and glucocorticoids. *Neuron* **11:**371–386.

Yang H and Chen C (2008) Cyclooxygenase-2 in synaptic signaling. *Curr Pharm Des* **14:**1443–1451.

Yu M, Ives D, and Ramesha CS (1997) Synthesis of prostaglandin E_2 ethanolamide from anandamide by cyclooxygenase-2. *J Biol Chem* **272:**21181–21186.

Address correspondence to: Sherrye T. Glaser, Department of Neurobiology and Behavior, Stony Brook University, Stony Brook, NY 11794-5230. E-mail: sherrye.glaser@stonybrook.edu